





Atmospheric pressure metal organic chemical vapor deposition of thin germanium films

Ronny Fritzsche^{1,3}, Dietrich R. Zahn^{2,3} , and Michael Mehring^{1,3,*} 

¹Fakultät für Naturwissenschaften, Institut für Chemie, Professur Koordinationschemie, Technische Universität Chemnitz, 09107 Chemnitz, Germany

²Fakultät für Naturwissenschaften, Institut für Physik, Professur Halbleiterphysik, Technische Universität Chemnitz, 09107 Chemnitz, Germany

³Center for Materials, Architectures and Integration of Nanomembranes (MAIN), TU Chemnitz, Rosenbergstraße 6, 09126 Chemnitz, Germany

Received: 13 October 2020

Accepted: 31 January 2021

Published online:

16 February 2021

© The Author(s) 2021

ABSTRACT

The deposition of thin germanium films by atmospheric pressure metal organic chemical vapor deposition at temperatures below 400 °C on substrates such as silicon wafers, float glass, and polyimide (Kapton®) using the diorganogermanes $\text{GeH}_2\text{Cp}^{4\text{M}}_2$ and $\text{GeH}_2\text{Cp}^*_2$ as molecular precursors is described. The deposition rates and thus the layer thicknesses can be varied by temperature and time to give layers with a thickness in the nanometer range. The homogeneity and roughness of the deposited films were analyzed by means of atomic force microscopy measurements showing the formation of smooth and uniform surfaces with roughnesses of the films in the range of (1 ± 0.15) nm to (4.5 ± 1.5) nm. Films with thicknesses between 50 and 750 nm were deposited and analyzed by Raman spectroscopy, vis-NIR spectroscopy, electron microscopy, energy dispersive X-ray spectroscopy (EDX), and X-ray photoelectron spectroscopy (XPS). The as-deposited films are composed of amorphous germanium containing approximately 10% of carbon. Using Kapton® as a substrate highly flexible films were obtained.

Introduction

With the development of new germanium-based functional materials for energy conversion [1], for lithium-ion batteries [2–11] or as photocatalysts [12], the synthesis of germanium nanorods, [13] nanowires

[14–19], and nanoparticles [20–26] has significantly gained in importance. In addition, germanium thin-films are of great interest with regard to potential applications, e.g., photovoltaics [27], plasmonics [28], optoelectronics [29], electronics [30–32], optics [28, 33], sensors [34, 35], and semiconductors [36, 37].

Handling Editor: Kevin Jones.

Address correspondence to E-mail: michael.mehring@chemie.tu-chemnitz.de

Therefore, diverse methods for the fabrication of germanium films such as thin-film transfer [38], AFM nanolithography [39], or laser photolysis techniques [40, 41] were reported, and in most cases, the deposition of films is addressed via the gas phase, *e.g.*, atomic layer deposition (ALD) [42], physical vapor deposition (PVD) [31, 43, 44], or metal organic chemical vapor deposition (MOCVD) [45–49]. While the production of nanoparticles and nanowires is nowadays a standard process and might be carried out under quite simple conditions, the deposition of films with thicknesses in the nanometer range requires complex equipment in form of CVD or PVD systems. The development of less expensive deposition processes with options for scaling-up using precursors adapted to this process will contribute to the further development of germanium-based functional materials.

Germanium tetrachloride was the first precursor for the deposition of germanium via a gas phase process [50], reported as early as 1887 by Winkler. He carried out the decomposition at high temperatures in the interior of a glass tube, forming a metallic mirror that was identified as germanium. In the following, a couple of precursors were developed, which can be divided into two groups; inorganic (carbon-free) and metal–organic (carbon-containing) precursors. Germanes such as GeH_4 [51, 52], Ge_2H_6 [53], or germanium itself, as used in electron beam evaporation or in the PVD process, belong to the compounds of the first group. They can be used to deposit high-purity films [36, 54] which hold potential in sensor [35] and semiconductor applications [36, 37]. The germanes are widely used for the deposition of films despite their high sensitivity to oxygen and water and the necessary high safety precautions. Further representatives of the inorganic germanium precursors are halogermanes such as GeI_2 [20, 55], GeI_4 [20], and GeCl_4 [56] which can be converted thermally [20] or under reductive conditions with hydrogen [57] into germanium films. In addition, Zintl phases such as CaGe_2 or MgGe were used as precursors for the deposition from solution [58], an approach which provided graphene-like materials [23, 58, 59] and nonporous germanium-based films [60].

Metal–organic germanium precursors belong to the second group of precursors, which are suitable for the deposition of germanium. If incorporation of carbon impurities in the final material does not

interfere with the intended application, they offer some advantages over the inorganic precursors. By introducing an organic ligand at germanium, the sensitivity to oxygen and water, the decomposition temperature, the solubility, and the volatility of the precursors can be controlled, which greatly improves their handling compared to inorganic precursors, especially with regard to those that are gaseous such as GeH_4 . Thus, organogermanes such as GeH_3tBu [45], GeVinyl_4 [46], GeH_3Blz [47], and GeH_3Cp^* [48] ($t\text{Bu} = \text{C}(\text{CH}_3)_3$; Vinyl = CHCH_2 ; Blz = $\text{CH}_2\text{C}_6\text{H}_5$; $\text{Cp}^* = \text{C}_5\text{Me}_5$) were demonstrated to be suitable for the deposition of germanium films. In particular, GeH_3Cp^* and $\text{GeH}_3\text{Cp}^{4\text{M}}$ ($\text{Cp}^{4\text{M}} = \text{C}_5\text{Me}_4\text{H}$) show a high potential due to their volatility and low decomposition temperature with regard to the production of germanium films, but so far they were accessible with rather low yield only [47, 48].

Our goal was to develop a simple CVD process using molecular precursors, that can be deposited at low temperatures, are less sensitive to air and hydrolysis and are accessible straightforward in high yields. The precursors of choice are the germanes $\text{GeH}_2\text{Cp}^{4\text{M}}_2$ (1, $\text{Cp}^{4\text{M}}$: tetramethylcyclopentadienyl) [47, 61] and $\text{GeH}_2\text{Cp}^*_2$ (2, Cp^* : pentamethylcyclopentadienyl) [62], which were briefly reported previously but in contrast to the monoorganogermanes GeH_3Cp^* and $\text{GeH}_3\text{Cp}^{4\text{M}}$ not tested for their usability in a CVD process. Here, we report on the deposition of thin films of germanium on float glass, silicon, and flexible polyimide foils (Kapton®) by atmospheric pressure metal organic chemical vapor deposition at temperatures below 400 °C starting from the organometallic molecular precursors $\text{GeH}_2\text{Cp}^{4\text{M}}_2$ (1) and $\text{GeH}_2\text{Cp}^*_2$ (2).

Results and discussion

Precursor synthesis and characterization

The chlorogermanes $\text{GeCl}_2\text{Cp}^{4\text{M}}_2$ and $\text{GeCl}_2\text{Cp}^*_2$ were prepared by salt metathesis reactions starting from GeCl_4 with two equivalents of the corresponding lithium salts LiC_5Me_5 and LiC_5HMe_4 , respectively (Scheme 1).

Hydrogenation of the chlorogermanes was carried out with LiAlH_4 and gave the corresponding dihydrides $\text{GeH}_2\text{Cp}^{4\text{M}}_2$ (1) and $\text{GeH}_2\text{Cp}^*_2$ (2) in nearly quantitative yields (1: 95%; 2: 98%). Compared with

the syntheses described in the literature of other molecular precursors such as GeH_2tBu_2 (reported yield: 6%) [63] and GeBzIh_3 (reported yield: 31%) [47], which were shown to be suitable for the deposition of germanium, the yields obtained for the dihydridogermanes **1** and **2** are significantly higher. The hydrogenation of the dichlorogermane $\text{GeCl}_2\text{Cp}^{4\text{M}}_2$ represents a significant improvement with regard to the synthesis as described in the literature, which is based on a disproportionation reaction of $\text{GeH}_3\text{Cp}^{4\text{M}}$ [47]. Noteworthy, the chlorogermanes are highly sensitive to moisture, while the hydrides **1** and **2** are only slightly sensitive to oxygen and water. They can be stored at 20 °C under argon for months without decomposition using normal glassware, while chlorogermanes need to be stored under inert atmosphere in sealed tubes.

In order to elucidate the potential of the precursors **1** and **2** for the deposition of germanium, both germanes were investigated with regard to their thermal behavior by means of Thermogravimetric Analysis (TGA), decomposition temperature measurements, and temperature-dependent PXRD measurements. The decomposition temperatures of **1** and **2** were determined to be 225 °C and 200 °C, respectively, which is significantly lower as compared to other tetravalent organogermanes such as GeVinyl_4 (dec. 450 °C), GeEt_4 (dec. 400 °C), or GeHEt_3 (dec. 350 °C) and thus are in the range as reported for divalent germanium precursors such as GeI_2 (dec. 210 °C to 300 °C) [20] and 1,3 di-tert-butyl-1,3,2-diazagermolidin-2-ylidines (dec. 140 °C) [64]. When heating the germanes **1** and **2** to 550 °C under inert conditions using a heating rate of 50 K/min, evaporation was observed and minor residues of 8.5% and 12.6% were obtained in case of **1** and **2**, respectively. The TGA residues were examined by means of EDX, and high germanium contents of 86.2% and 89.3% in case of **1** and **2**, respectively, were detected, while carbon (9.4–11.0%) and oxygen (1.3–2.8%) represent only minor impurities. In temperature-dependent PXRD measurements in sealed quartz glass capillaries starting from the pure germanes **1** and **2** reflections for

crystalline germanium are observed at approximately 500 °C. It is thus assumed that the decomposition of the precursor provides amorphous germanium first, which then crystallizes at 500 °C. It should be noted that the crystallization temperature of germanium significantly depends on purity and annealing conditions [65, 66], however, a significantly lower crystallization temperature of the amorphous germanium in the range 300 °C to 400 °C was expected [67].

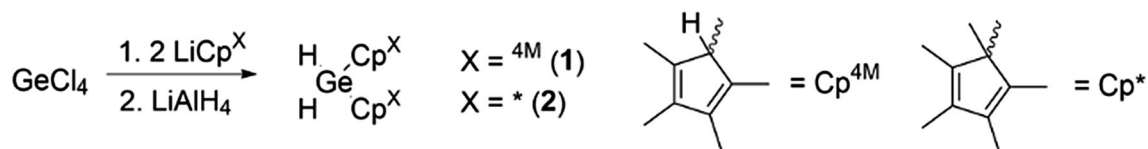
In conclusion, both germanes **1** and **2** are easily accessible, easy to handle, show high volatility and low decomposition temperatures. For these reasons, the two germanes were chosen as promising candidates for the development of a simple AP MOCVD process for the production of thin and flexible germanium films.

Experimental setup for the deposition of germanium films

The deposition setup (Fig. 1) is kept simple and does not require vacuum, plasma, gas flow, or cooling traps which are usually required for the CVD process. The apparatus consists of three parts: i) the evaporator vessel, which here is a silver crucible containing the precursor; ii) a holder made of copper wire, which carries the evaporation vessel; iii) a glass vessel with a flat opening, which serves as the reactor and is placed on the substrate. The experimental setup is placed on a ceramic heater, which at best but not necessarily is located in a glove box under inert gas. The maximum temperature used for the deposition on float glass, and silicon wafers was set to 550 °C, whereas the maximum temperature for the deposition on Kapton® was set to 400 °C.

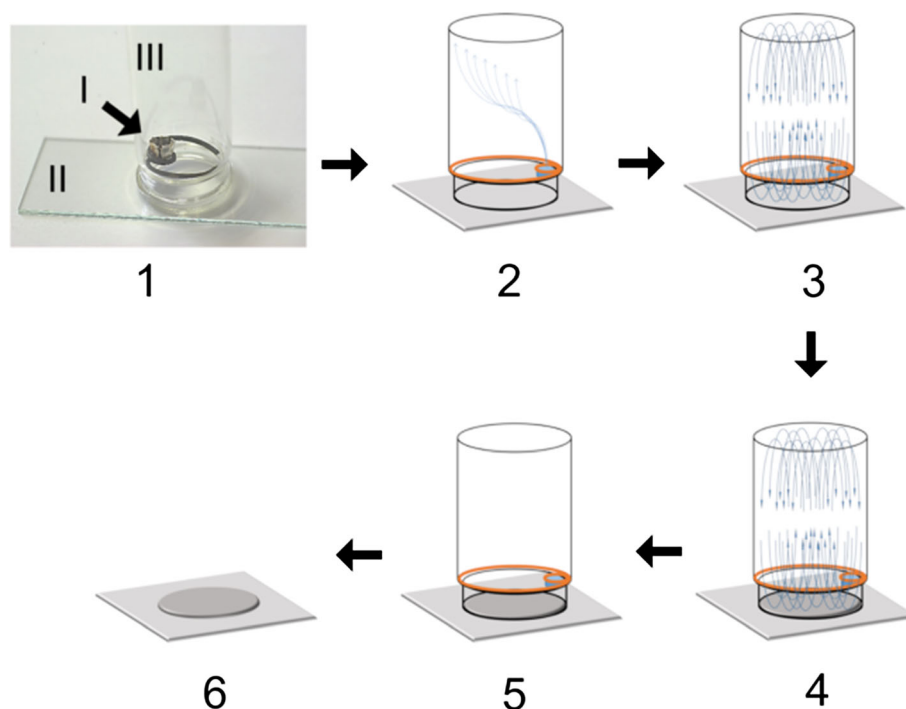
Characterization of the germanium films

For the deposition experiments silicon wafers with a natural SiO_2 film, float glass and Kapton® were chosen. These substrates provide adequate thermal stability for the deposition, a smooth surface with a roughness < 0.5 nm, and are chemically resistant to



Scheme 1 Reaction scheme for the synthesis of diorganogermanes $\text{GeH}_2\text{Cp}^{4\text{M}}_2$ (**1**) and $\text{GeH}_2\text{Cp}^*_2$ (**2**).

Figure 1 Schematic sequence of the AP CVD process for the deposition of germanium: 1 Arrangement for the deposition of germanium films on the substrate, here float glass; 2 Heating of the apparatus and thus evaporation of the precursor; 3 Formation of a convective flow within the reactor; 4 Decomposition and thin film formation at the surface of the substrate; 5 Condensation of volatile decomposition products in the upper region of the reactor; 6 Removal of the reactor and thermal evaporation of residual organics.



the solvents used for cleaning the surfaces (acetone, ethanol, and Et_2O).

In an initial step, several experiments were carried out in order to determine the minimum substrate temperature necessary for the deposition starting from both precursors. The most important requirement at this stage was that the film adheres to the substrate, which was tested using a standardized Scotch tape test of the American Society for Testing and Materials (ASTM D3359-17). The substrate temperature was successively increased in steps of 5 K beginning at 250 °C. A temperature of 270 °C for 1 and 260 °C for 2 was determined as the lowest applicable deposition temperature. At deposition temperatures higher than 350 °C for 2 and 400 °C for 1 inhomogeneous films on all selected substrates, which partially peeled off from the substrate, were observed. Thus, the optimum temperature window for the deposition process ranges from 275 °C up to 350 °C for 2 and from 280 °C to 400 °C for 1. The closed setup is advantageous in that a high concentration of the precursor is present in the gas phase, as previously described by Harrison et al. for tetravinylgermane [46]. Figure 2 shows two deposited germanium films on float glass and Kapton® deposited by our AP MOCVD method. Noteworthy, germanium films deposited on Kapton® are flexible and permit to apply a bending radius below 2 mm

without the germanium films chipping off from the substrate and without cracking (Fig. 3).

In the simple setup a roll rim glass was used, but scaling-up is easily possible. Germanium films with a diameter of up to 11 cm were fabricated using glass reactors of larger diameter. However, in the experiments as described in the following commercially available 10 mL roll rim glasses with a neck diameter of 18 mm were used.

For a more detailed characterization of the thin germanium films scanning electron microscopy (SEM), energy dispersive X-ray spectroscopy (EDX), X-ray photoelectron spectroscopy (XPS), and Raman spectroscopy were used. Deposition on silicon wafers was carried out for 3 min at 275 °C, 300 °C, and 325 °C with 2, respectively, at 300 °C, 325 °C, and 350 °C with 1. The as-deposited films were characterized using Raman spectroscopy. All samples revealed similar and characteristic spectra showing broad bands with peak maxima at 265–273 cm^{-1} , which is characteristic for amorphous germanium (Fig. 4). Despite the presence of carbon distinct bands for carbon were not observed, and only the humps at 1500–1600 cm^{-1} might indicate carbon residues. Noteworthy, the films might be easily crystallized using laser-induced crystallization. We did observe that a symmetric Raman band at 294 cm^{-1} evolved upon measuring the Raman spectra for more than

Figure 2 Deposited germanium films on Kapton® (left) and glass (right) (circle diameter 18 mm, precursor 1, deposition temperature: 300 °C).

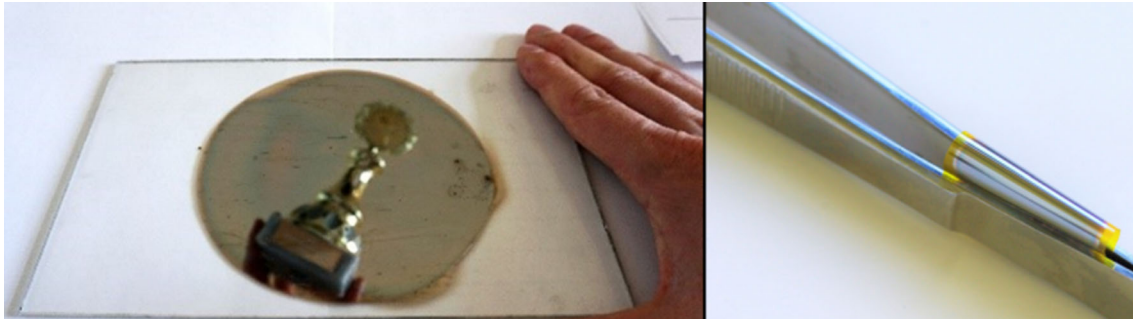
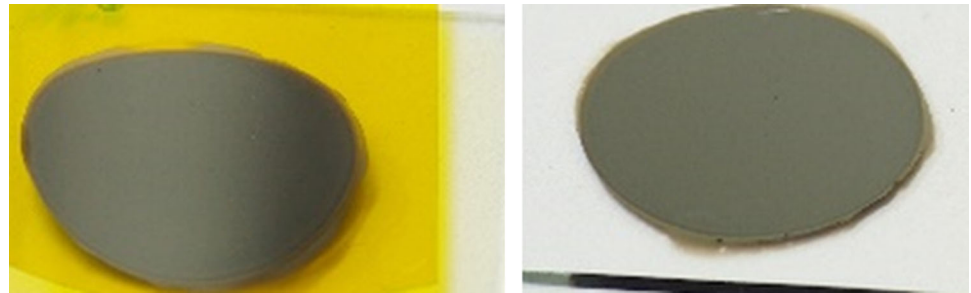


Figure 3 Deposited flexible germanium films on float glass with a circle diameter of 110 mm (left) and on Kapton® with a circle diameter of 18 mm (right) starting from germane 1.

30 s using an Argon Laser with a wavelength of 514.5 nm, which is indicative for the beginning of crystallization. However, as the phonon frequency of crystalline Ge is 300 cm^{-1} the shift to 294 cm^{-1} shows the formation of small crystallites. Moreover, the remaining broad feature at lower frequency indicates that the crystallization is not complete, which is in line with previous studies on hydrogenated carbon germanium films (Fig. 5) [68].

Figure 6 (left) shows the SEM cross-section of the sample, that was prepared by deposition of 1 at 350 °C on a silicon wafer. Here, the germanium film (red frame) deposited on the silicon wafer is well visible, and EDX proofs the deposition a germanium-rich film on the silicon wafer.

In addition to surface analysis, the deposited film was analyzed using XPS before and after sputtering, whereby approximately 30 nm of the films was removed (Fig. S1–S12). At the surface, all samples exhibited oxygen and carbon in addition to germanium. Regardless of the precursor and the deposition temperature carbon contents in the range of 20–30% were observed. The high oxygen content of 25–31% most likely results from a native germanium dioxide layer. This assumption is confirmed by the fact that the sputtered samples did not reveal any oxygen. However, even the sputtered samples and thus the

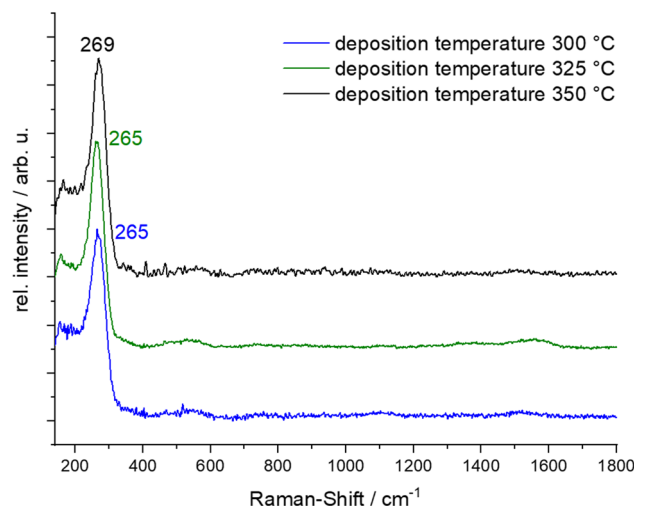


Figure 4 Raman spectra of the germanium films deposited on silicon wafers starting from 1.

bulk material contain significant amounts of carbon (10 – 15%) [69]. In conclusion, our deposition experiments revealed two trends: (i) at higher deposition temperatures the amount of incorporated carbon is lower and (ii) the Cp* substituted germane 2 gives slightly lower carbon contents at the same deposition temperature as used for Cp^{4M} substituted 1 despite an increased carbon content in the precursor. The lowest carbon contents were found for deposition of 2

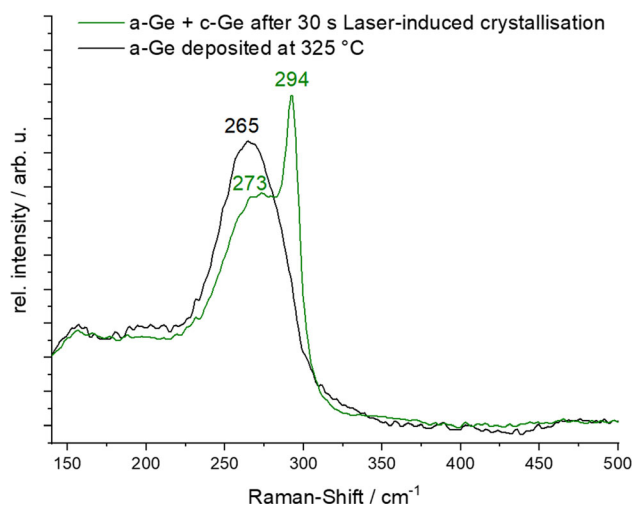


Figure 5 Raman spectra of germanium films deposited from germane **1** before (black line) and after 30 s (green line) laser-induced crystallization.

at 325 °C (10.6%) and for deposition of **1** at 350 °C (11.5%).

Thickness determination of the as-deposited films

Atomic force microscopy (AFM) was used to determine the film thickness and the surface texture of the deposited germanium films on solid substrates such as float glass and silicon. Therefore, a stainless steel needle is used to scratch the germanium film on the substrate, and the measurement is carried out at the thus produced edge. The thickness as well as the surface roughness is determined in a single measurement at the edge (method A, for details see ESI Fig. S13). For both precursors, it is observed that the film thickness does not significantly depend on the precursor used and increases with increasing temperature while using a constant deposition time of three minutes. The final deposited films are quite similar in thickness for both precursors (113 nm–120 nm) when a temperature of 300 °C is applied.

Table 1 Film thickness of films deposited on Si wafers at 325 °C starting from **1** as a function of time at different positions X (distance from the edge: X1: 5 mm; X2: 2.5 mm; X3: 1 mm)

Time/min	X1/nm	X2/nm	X3/nm	Variation/%
1	157	143	137	7.8
2	215	211	205	2.2
3	310	293	285	4.7
4	363	360	341	2.4

However, at 275 °C film deposition was not observed using precursor **1** and at 350 °C homogeneous films were only obtained from precursor **2**. In the following, we concentrated our work on compound **1**, which offers a better synthetic availability.

In order to check the homogeneity of the deposited films using different time intervals, germanium films starting from **1** were deposited at 325 °C in time intervals of one minute up to four minutes. The film thickness determination was carried out at three positions of the substrate using method A, [distance from the edge: X1: 5 mm; X2: 2.5 mm; X3: 1 mm from the edge (Table 1)]. All samples show only a small variation of the film thickness (2.2% to 7.8%) when comparing the thickness at the center with the film thickness at outer parts of the Si wafer.

In addition to the film thickness, the morphology and roughness R_{RMS} (RMS—root-mean-squared) of the as-deposited films (deposition time: 3 min) were investigated using AFM. With respect to the morphology, the AFM images of films show a characteristic grain size (Fig. 7), which reaches from a few to 200 nm depending on the deposition temperature and is similar to that observed for germanium films deposited by low pressure CVD or epitaxy [27, 54, 70]. As the deposition temperature increases, an increase in the diameter of the individual grains at the surface is observed. The specific roughness of the films is between (1 ± 0.15) nm and (4.5 ± 1.5) nm for

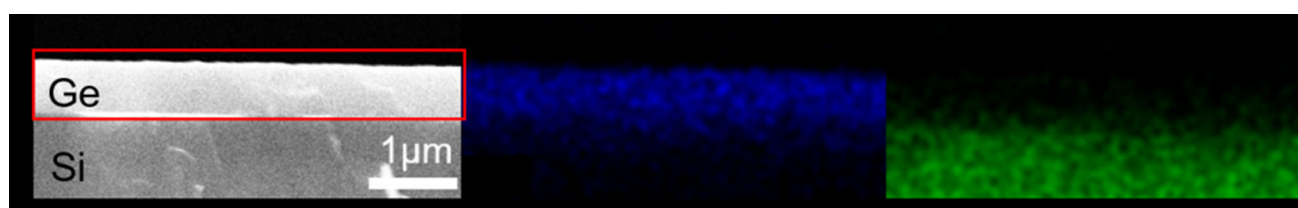


Figure 6 SEM cross-section (left) of a germanium film on silicon and EDX images of Ge (middle), and Si (right); film deposited starting from **1**.

Figure 7 AFM images of the surfaces of germanium films deposited on float glass at 375 °C (left) and 300 °C (right) starting from precursor 1.

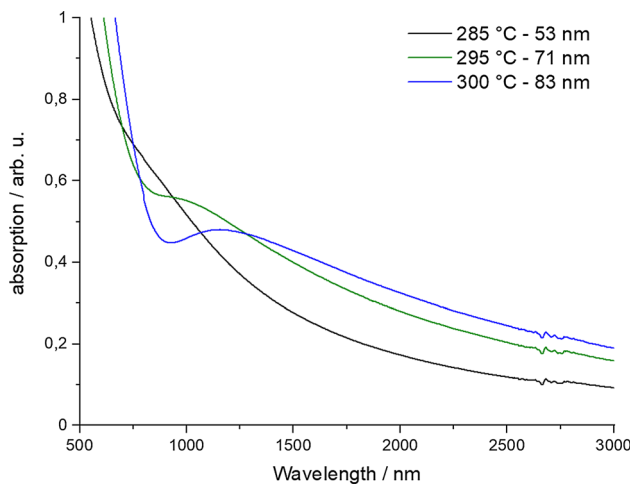
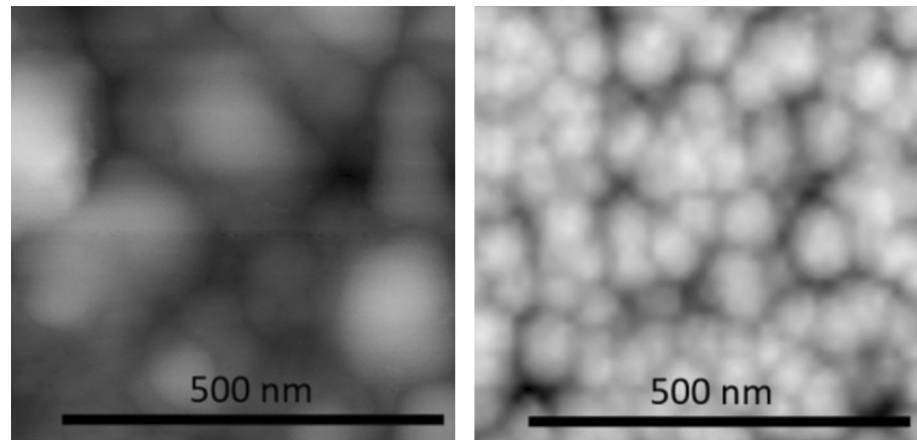


Figure 8 Development of the first-order absorption minima in the vis–NIR spectra at 53–83 nm thick films of germanium on float glass as-deposited starting from 1 at various temperatures (deposition time 3 min).

films deposited at 275 °C and 400 °C, respectively. The roughness increases with increasing deposition temperature, deposition rate, and film thickness. With regard to the morphology and roughness, the germanium films deposited at temperatures below 300 °C are comparable with germanium films deposited by means of CVD using GeH_4 or magnetron sputtering using Ge targets [27, 54, 70].

Due to the optical properties of thin germanium films, it is possible to determine the film thickness by vis–NIR measurements (Figs. 8–10) as was demonstrated recently [71]. This method is particularly interesting, since in contrast to AFM studies the film is not destroyed for or by the measurement (method B). For the film thickness determination, the interference effect is used as described for a Fabry–Pérot

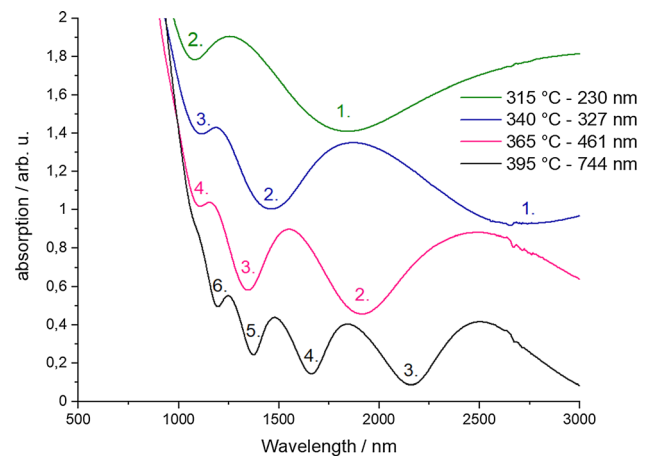


Figure 9 Film thickness dependence of absorption minima of germanium films on float glass as-deposited starting from 1 at various temperatures (deposition time 3 min); second order (green curve 230 nm), third order (blue curve 327 nm), fourth order (pink curve 461 nm), and sixth order (black curve 744 nm).

interferometer. The reflection of the irradiated light within the film at the interfaces germanium–glass and germanium–air is used. Within the film, constructive and destructive interference occur depending on the irradiated wavelength and the film thickness. Thus, the position of the transmission maxima depends on the film thickness, which then is calculated by $2 \cdot n \cdot d = m \cdot \lambda_{\min}$. For this purpose, the refractive index of germanium is used for variable n at λ_{\min} (minimum absorption) [72], d is the film thickness to be determined, m is the order of the interference (integer), and λ_{\min} corresponds to the wavelength with minimal absorption.

The film thicknesses of Ge on float glass determined by means of vis–NIR spectroscopy are plotted as a

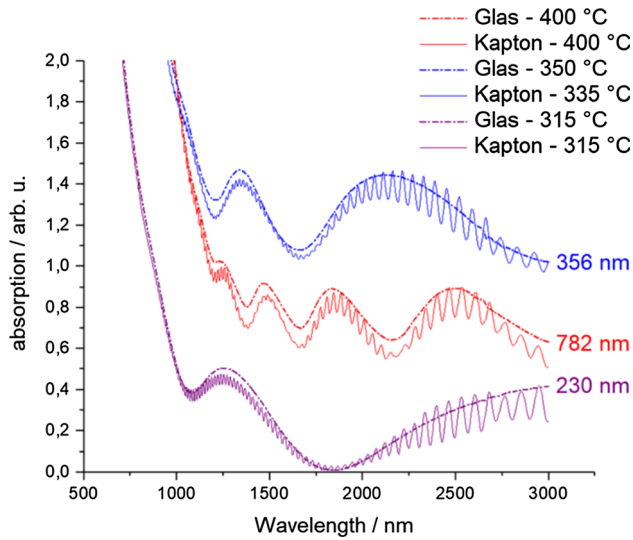


Figure 10 Germanium films as-deposited starting from **1** on float glass (dotted line) and Kapton® (solid line) at various temperatures (deposition time 3 min).

function of deposition temperature (Figs. 11 and 12). The comparison shows a very good agreement of the values determined by means of vis-NIR spectroscopy (non-destructive method B) with the values determined from the AFM measurements (destructive method A).

The film thickness of deposited films on float glass was additionally determined using method A: center at 0 mm, at ± 4.5 mm distance from the center, and at ± 7.5 mm distance from the center. By this, we get an idea of the uniformity of the film deposition at different temperatures (deposition time: 3 min) on

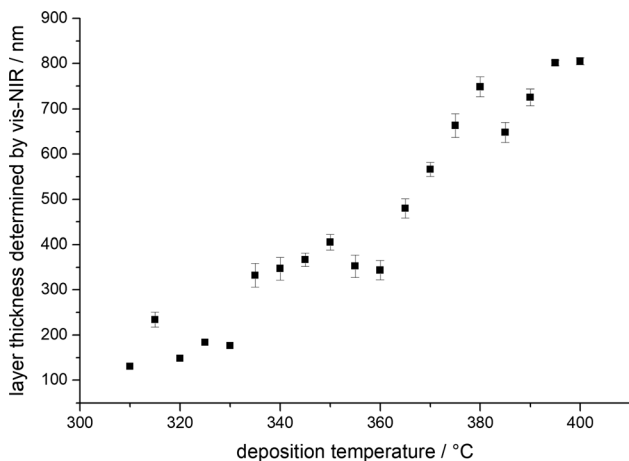


Figure 11 Film thickness of Ge on float glass as determined by vis-NIR measurements (method B) vs. temperature (deposition time: 3 min).

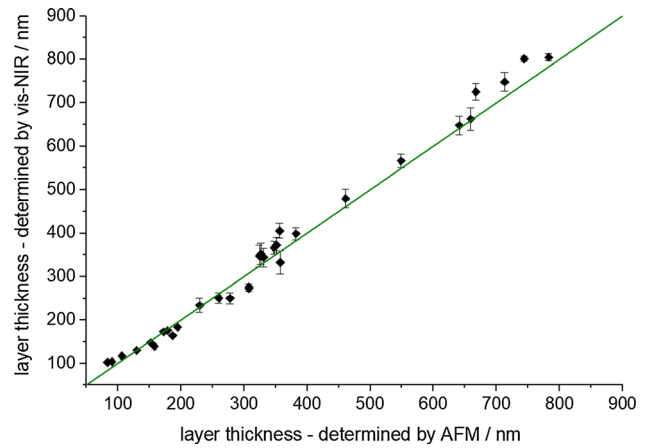


Figure 12 Correlation of the layer thickness of Ge on float glass determined by AFM (method A) and vis-NIR (method B), green line represents the $f(x) = x$ function.

the example of precursor **1** (Fig. 13). At temperatures below 330 °C, quite uniform films were deposited and a linear correlation of deposition temperature and film thickness is observed. In a second temperature regime from 335 °C to 360 °C, a film thickness of approximately 300 nm is obtained, regardless of the temperature, and the films appear to be less uniform. At higher temperatures the film thickness again increases but also the deviation increases significantly and thus non-uniform films are obtained. Methods A and B provide similar results.

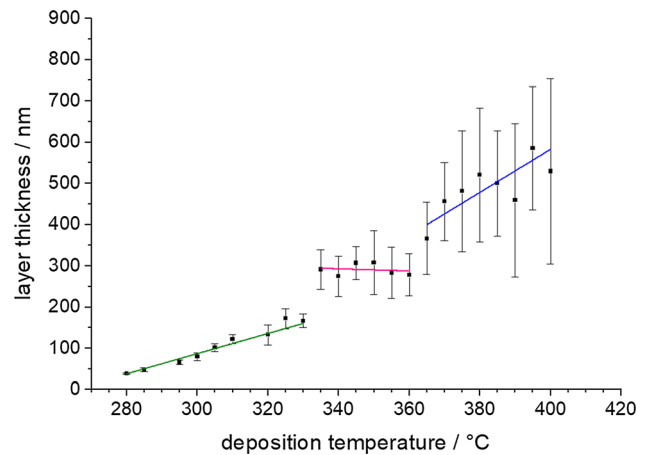


Figure 13 Dependence of the germanium film thickness using a constant deposition time starting from precursor **1** (temperature range: 280–400 °C, deposition time: 3 min; substrate: float glass). The standard deviation was determined based on measurements of the film thickness at five positions of the substrate (center at 0 mm, at ± 4.5 mm distance from the center, and at ± 7.5 mm distance from the center).

The observed deposition characteristics are well in line with common CVD process parameters. A characteristic relationship between film growth and substrate temperature is observed, which can be divided into three processes: i) kinetically controlled film growth at low temperatures; ii) stagnation of the film growth in a certain temperature range as a result of saturation of the surface with the precursor; iii) an increase of the deposition rate by premature decomposition of the precursor in the gas phase. With regard to this, we analyzed the deposition process of our setup using an Arrhenius plot (Fig. 14).

In the temperature range between 280 °C to 330 °C (Fig. 14 green line), an increase in the deposition rate is observed with increasing temperature. Extrapolation would give an intersection with the y-axis at about 222 °C, which marks the beginning of the film deposition. This value correlates well with the experimentally determined decomposition temperature of 225 °C of precursor **1**. The deposited films show a uniform film thickness. The film growth is kinetically controlled in this temperature regime, and the activation energy of the thermal decomposition of the precursor **1** was determined from the Arrhenius Plot to amount to 101 kJ/mol (Fig. 14). This value is significantly lower as reported for other organogermanium(IV) precursors (GeEt_4 142 kJ/mol [73], GeH_3tBu 160 kJ/mol [45], and GeVinyl_4 185 kJ/mol [46]). The digermane Ge_2H_6 also shows a higher activation energy of 125 kJ/mol at 0.0039 mbar and 163 kJ/mol at 0.295 mbar [74]. The only report for a lower activation energy is given by Veprek et al. for

3-di-tert-butyl-1,3,2-diazagermolidin-2-ylidene, which shows an activation energy of 90 kJ/mol. However, this precursor follows a disproportionation reaction, and thus a maximum of 50% of the germanium might be deposited [64]. The low activation energy for the decomposition of **1** confirms that $\text{Cp}^{4\text{M}}$ is easily cleaved off, and the corresponding diorganogermane is suitable for the deposition of germanium at low temperatures. In the second temperature range between 330 °C to 360 °C (Fig. 14 pink line), there is no further increase in the deposition rate, and the latter remains constant, which is explained by a diffusion controlled process and surface saturation with precursor **1**. Films deposited in this temperature regime were roughly (290 ± 15) nm thick. In the third temperature range, 365 °C to 400 °C (Fig. 14 blue line), an irregular increase in the deposition rate occurs. The deposition is inhomogeneous starting from 365 °C. A film thickness of (455 ± 95) nm was determined at 370 °C and films deposited at 400 °C showed a thickness of (529 ± 224) nm. Here the precursor decomposes prematurely in the gas phase, but still contributes to film growth (Fig. 14). In a classical CVD system, a continuous gas stream removes the precursor that is decomposed in the gas phase, and thus, they do not contribute to the growth of the film.

Conclusions

A simple and efficient atmospheric pressure metal-organic chemical vapor deposition process (AP MOCVD) was developed for the formation of thin germanium films starting from the diorganogermanes $\text{GeH}_2\text{Cp}^{4\text{M}}_2$ [75] and $\text{GeH}_2\text{Cp}^*_2$ [62, 75] as molecular precursors. Deposition temperatures below 350 °C are sufficient to produce uniform deposition on substrates such as silicon wafers, float glass, and polyimide (Kapton®). Deposition on Kapton® provides highly flexible Ge films. The deposition rates and thus the layer thickness can be varied by temperature and time to give amorphous germanium films with a thickness in the nanometer range. Previously, the use of monoorganogermanes was favored because the probability of incorporation of high amounts of carbon was thought to be reduced in comparison to precursors based on diorganogermanium compounds. We observe carbon incorporation into the films with approximately 10%, a value

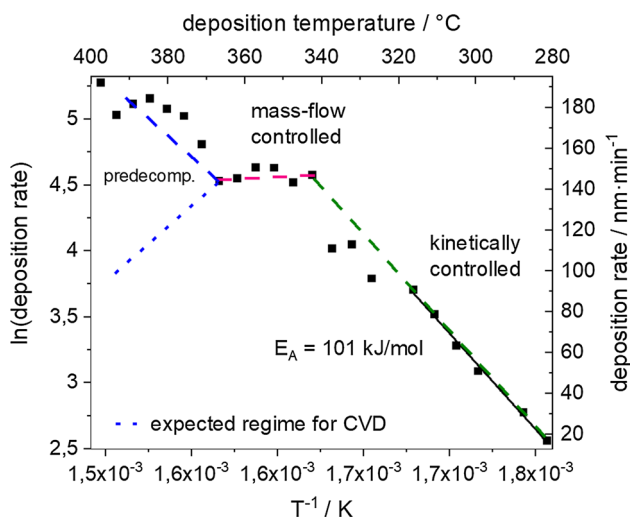


Figure 14 Arrhenius plot for the deposition of precursor **1** on float glass.

which is comparable to films prepared from monoorganogermanium precursors. Thus, carbon incorporation seems to be strongly depending on process parameters rather than on composition of the organogermanium precursor. The presented process is highly valuable when carbon contamination does not interfere with the envisaged application and when amorphous and flexible germanium films are the synthetic target, especially when temperatures of 350 °C should not be exceeded and when the process should be kept simple. The molecular precursors show sufficient volatility and are easy to handle because of their significantly reduced sensitivity towards oxygen and moisture as compared to germanes of the type $RGeH_3$ or GeH_4 .

Experimental section

Melting points (sealed off in argon flushed capillaries) were determined using a Büchi Melting Point B-540. Raman spectra were measured with a HORIBA LabRAM HR800 with Argon Laser (Wavelength: 514.5 nm), Objective: 100 x, power density 1 mW and an integration time of 30 s. Vis–NIR measurements were carried out using a Varian Cary 5000 UV–Vis–NIR spectrometer. AFM measurements were carried out using a JPK NanoWizard (JPK Instruments AG, Berlin). SEM/EDX analysis were determined with a FEI NovaNano SEM. Powder X-ray diffraction was carried out with a STOE STADI P diffractometer (Darmstadt, Germany) using $CuK\alpha_1$ radiation ($\lambda = 1.54056$ nm, 40 kV, 40 mA) and a Ge(111)-monochromator. The FWHM is corrected for instrumental broadening using a LaB_6 standard (SRM 660) purchased from NIST. TGA experiments were determined by using a Mettler Toledo TGA/DSC1 1100 system. The measurements were performed in a temperature range from 30 to 550 °C with a rate of $10\text{ K} \cdot \text{min}^{-1}$ and a nitrogen volume flow of $20\text{ mL} \cdot \text{min}^{-1}$.

Depositions

A series of samples of germanium films was produced using the diorganogermanium precursors on Kapton® and float glass as substrates. The deposition of the germanium films was carried out at a substrate temperature of 280 °C and was increased by 5 °C to 400 °C for each new sample. The deposition of

germanium on a silicon substrate was carried out at 350 °C using the precursor $GeH_2Cp^{4M}_2$. A deposition time of 3 min was chosen unless otherwise described.

All experiments were carried out at atmospheric pressure in a glove box under a nitrogen atmosphere (oxygen and water content < 0.5 ppm) using a computer-controlled ceramic heating plate (Bath Resistor Ceramics). The temperature of the heating plate can be varied between 25 and 550 °C. The substrates used were float glass (25 × 80 mm) from VWR Collection, silicon wafer with a natural oxide film (10 × 10 mm), or Kapton® 100 QR 2 films (25 × 25 × 0.025 mm) from DuPont. All substrates were treated with acetone, ethanol, and diethylether for 3 min in an ultrasonic bath before the deposition experiments and then dried at 120 °C. As evaporation vessels, home-build silver crucibles made of silver foil (\varnothing approx. 5 mm, height-7-mm, thickness-0.1-mm) were used. Unless otherwise described, all deposition experiments were performed with 10.0 ± 0.3 mg of the precursors $GeH_2Cp^{4M}_2$ (1) [75] and $GeH_2Cp^*_2$ (2), which we prepared according to literature procedures [62, 75].

Acknowledgements

Open Access funding enabled and organized by Projekt DEAL. This publication contains parts including revised versions of the schemes, tables, and figures of the PhD thesis “Einsatz von Methylcyclopentadienyl-substituierten Silanen und Germanen zur Synthese verbrückter Heterozyklen und zur Abscheidung von dünnen Germaniumschichten“ of Ronny Fritzsche published in 2017 at Technische Universität Chemnitz [75]. We are grateful to the Bundesministerium für Bildung und Forschung, the Sächsisches Staatsministerium für Wissenschaft und Kunst and TU Chemnitz for financial support. We are grateful to Diana Voigt, Natalia Rüffer, Dunja Grimm and Marcus Weber for performing the AFM, TGA, and Raman measurements, respectively. Daniel Lehmann is gratefully acknowledged for XPS measurements and discussion. We thank Ana-Maria Fritzsche for discussion and assistance of manuscript editing.

Funding

This study was funded in part by the Bundesministerium für Bildung und Forschung (BMBF; Project

No. 214648) and the Sächsisches Staatsministerium für Wissenschaft und Kunst (SMWK, Project No. 4-7531.50/1128/1).

Compliance with ethical standards

Conflict of interest The authors declare that they have no conflict of interest.

Supplementary Information: The online version contains supplementary material available at <http://doi.org/10.1007/s10853-021-05871-9>.

Open Access This article is licensed under a Creative Commons Attribution 4.0 International License, which permits use, sharing, adaptation, distribution and reproduction in any medium or format, as long as you give appropriate credit to the original author(s) and the source, provide a link to the Creative Commons licence, and indicate if changes were made. The images or other third party material in this article are included in the article's Creative Commons licence, unless indicated otherwise in a credit line to the material. If material is not included in the article's Creative Commons licence and your intended use is not permitted by statutory regulation or exceeds the permitted use, you will need to obtain permission directly from the copyright holder. To view a copy of this licence, visit <http://creativecommons.org/licenses/by/4.0/>.

References

- [1] Barth S, Hernandez-Ramirez F, Holmes JD, Romano-Rodriguez A (2010) Synthesis and applications of one-dimensional semiconductors. *Prog Mater Sci* 55:563
- [2] Jin S, Li N, Cui H, Wang C (2014) Embedded into graphene Ge nanoparticles highly dispersed on vertically aligned graphene with excellent electrochemical performance for lithium storage. *ACS Appl Mater Interfaces* 6:19397
- [3] Liang W, Yang H, Fan F et al (2013) Tough germanium nanoparticles under electrochemical cycling. *ACS Nano* 7:3427
- [4] Sun Y, Jin S, Yang G, Wang J, Wang C (2015) Germanium nanowires-in-graphite tubes via self-catalyzed synergetic confined growth and shell-splitting enhanced Li-storage performance. *ACS Nano* 9:3479
- [5] Xiao Y, Cao M (2014) High-performance lithium storage achieved by chemically binding germanium nanoparticles with N-doped carbon. *ACS Appl Mater Interfaces* 6:12922
- [6] Xu Y, Zhu X, Zhou X et al (2014) Ge nanoparticles encapsulated in nitrogen-doped reduced graphene oxide as an advanced anode material for lithium-ion batteries. *J Phys Chem C* 118:28502
- [7] Li D, Wang H, Liu HK, Guo Z (2016) A new strategy for achieving a high performance anode for lithium ion batteries—Encapsulating germanium nanoparticles in carbon nanoboxes. *Adv Energy Mater* 6:1501666
- [8] Hao J, Yang Y, Zhao J et al (2017) Ionic liquid electrodeposition of strain-released germanium nanowires as stable anodes for lithium ion batteries. *Nanoscale* 9:8481
- [9] Kim C, Song G, Luo L et al (2018) Stress-Tolerant nanoporous germanium nanofibers for long cycle life lithium storage with high structural stability. *ACS Nano* 12:8169
- [10] Liu X, Lin N, Cai W et al (2018) Mesoporous germanium nanoparticles synthesized in molten zinc chloride at low temperature as a high-performance anode for lithium-ion batteries. *Dalton Trans* 47:7402
- [11] Kim T-H, Song H-K, Kim S (2019) Production of germanium nanoparticles via laser pyrolysis for anode materials of lithium-ion batteries and sodium-ion batteries. *Nanotechnology* 30:275603
- [12] Liu Z, Lou Z, Li Z et al (2014) GeH: a novel material as a visible-light driven photocatalyst for hydrogen evolution. *Chem Commun* 50:11046
- [13] Chockla AM, Harris JT, Korgel BA (2011) Colloidal synthesis of germanium nanorods. *Chem Mater* 23:1964
- [14] Lu X, Harris JT, Villarreal JE, Chockla AM, Korgel BA (2013) Enhanced nickel-seeded synthesis of germanium nanowires. *Chem Mater* 25:2172
- [15] Mullane E, Kennedy T, Geaney H, Dickinson C, Ryan KM (2013) Synthesis of tin catalyzed silicon and germanium nanowires in a solvent-vapor system and optimization of the seed/nanowire interface for dual lithium cycling. *Chem Mater* 25:1816
- [16] Geaney H, Mullane E, Ryan KM (2013) Solution phase synthesis of silicon and germanium nanowires. *J Mater Chem C* 1:4996
- [17] Kim BJ, Wen CY, Tersoff J, Reuter MC, Stach EA, Ross FM (2012) Growth pathways in ultralow temperature Ge nucleation from Au. *Nano Lett* 12:5867
- [18] Toko K, Nakata M, Jevasuwan W, Fukata N, Suemasu T (2015) Vertically aligned Ge nanowires on flexible plastic films synthesized by (111)-oriented Ge seeded vapor–liquid–solid growth. *ACS Appl Mater Interfaces* 7:18120
- [19] O'Regan C, Biswas S, Petkov N, Holmes JD (2014) Recent advances in the growth of germanium nanowires: synthesis, growth dynamics and morphology control. *J Mater Chem C* 2:14

- [20] Muthuswamy E, Iskandar AS, Amador MM, Kauzlarich SM (2013) Facile synthesis of germanium nanoparticles with size control: microwave versus conventional heating. *Chem Mater* 25:1416
- [21] Zaitseva N, Dai ZR, Grant CD, Harper J, Saw C (2007) Germanium nanocrystals synthesized in high-boiling-point organic solvents. *Chem Mater* 19:5174
- [22] Rao CNR, Ramakrishna Matte HSS, Voggu R, Govindaraj A (2012) Recent progress in the synthesis of inorganic nanoparticles. *Dalton Trans* 41:5089
- [23] Vaughn DD II, Schaak RE (2013) Synthesis, properties and applications of colloidal germanium and germanium-based nanomaterial. *Chem Soc Rev* 42:2861
- [24] Lu XM, Ziegler KJ, Ghezelbash A, Johnston KP, Korgel BA (2004) Synthesis of germanium nanocrystals in high temperature supercritical fluid solvents. *Nano Lett* 4:969
- [25] Vaughn DD, Bondi JF, Schaak RE (2010) Colloidal synthesis of air-stable crystalline germanium nanoparticles with tunable sizes and shapes. *Chem Mater* 22:6103
- [26] Carolan D (2017) Recent advances in germanium nanocrystals: Synthesis, optical properties and applications. *Prog Mater Sci* 90:128
- [27] Tsao C-Y, Weber JW, Campbell P, Widenborg PI, Song D, Green MA (2009) Low-temperature growth of polycrystalline Ge thin film on glass by in situ deposition and ex situ solid-phase crystallization for photovoltaic applications. *Appl Surf Sci* 255:7028
- [28] Frigerio J, Ballabio A, Isella G et al (2016) Tunability of the dielectric function of heavily doped germanium thin films for mid-infrared plasmonics. *Physical Review B* 94:085202
- [29] Lee W-J, Sharp J, Umana-Membreno GA, Dell J, Faraone L (2015) Investigation of crystallized germanium thin films and germanium/silicon heterojunction devices for optoelectronic applications. *Mater Sci Semicond Process* 30:413
- [30] Toko K, Nakao I, Sadoh T, Noguchi T, Miyao M (2009) Electrical properties of poly-Ge on glass substrate grown by two-step solid-phase crystallization. *Solid-State Electron* 53:1159
- [31] Nassar JM, Hussain AM, Rojas JP, Hussain MM (2014) Low-cost high-quality crystalline germanium based flexible devices. *Physica Status Solidi (RRL) Rapid Res Lett* 08:794
- [32] Liao C, Chen S, Huang W, Shen C, Shieh J, Cheng H (2018) High-performance recessed-channel germanium thin-film transistors via excimer laser crystallization. *IEEE Electron Device Lett* 39:367
- [33] Esther ACM, Dey A, Sridhara N et al (2015) A study on degradation of germanium coating on Kapton used for spacecraft sunshield application. *Surf Interface Anal* 47:1155
- [34] Ho WS, Dai YH, Deng Y et al (2009) Flexible Ge-on-polyimide detectors. *Appl Phys Lett* 94:3
- [35] Prucnal S, Liu F, Voelskow M et al (2016) Ultra-doped n-type germanium thin films for sensing in the mid-infrared. *Sci Rep* 6:27643
- [36] Soriano V, Colace L, Armani N et al (2011) Low-temperature germanium thin films on silicon. *Opt Mater Express* 1:856
- [37] Goley PS, Hudait MK (2014) Germanium based field-effect transistors: Challenges and opportunities. *Materials* 7:2301
- [38] Maeda T, Ishii H, Itatani T et al (2013) Ultrathin layer transfer technology for post-Si semiconductors. *Microelectron Eng* 109:133
- [39] Torrey JD, Vasko SE, Kapetanovic A, Zhu Z, Scholl A, Rolandi M (2010) Scanning probe direct-write of germanium nanostructures. *Adv Mater* 22:4639
- [40] Pola J, Parsons JP, Taylor R (1992) Deposition of germanium by laser-induced photolysis of organogermanes in the liquid-phase. *J Mater Chem* 2:1289
- [41] Lollmahomed F, Leigh WJ (2009) Laser flash photolysis studies of some dimethylgermylene precursors. *Organometallics* 28:3239
- [42] Kim SB, Sinsermsuksakul P, Hock AS, Pike RD, Gordon RG (2014) Synthesis of N-heterocyclic stannylene (Sn(II)) and germylene (Ge(II)) and a Sn(II) amidinate and their application as precursors for atomic layer deposition. *Chem Mater* 26:3065
- [43] Cavalcoli D, Impellizzeri G, Romano L, Miritello MP, Grimaldi MG, Fraboni B (2015) Optical properties of nanoporous germanium thin films. *ACS Appl Mater Interfaces* 7:16992
- [44] Hussain AM, Fahad HM, Sevilla GAT, Hussain MM (2013) Thermal recrystallization of physical vapor deposition based germanium thin films on bulk silicon (100). *Physica Status Solidi (RRL) Rapid Res Lett* 7:966
- [45] Suda K, Kijima T, Ishihara S et al (2015) Growth of Ge homoepitaxial films by metal-organic chemical vapor deposition using *t*-C₄H₉GeH₃. *ECS J Solid State Sci Technol* 4:P152
- [46] Harrison PG, de Cointet C, Podesta DM et al (1994) Pre-deposition chemistry underlying the formation of germanium films by CVD of tetravinylgermane. *Chem Mater* 6:1620
- [47] K Dittmar (2002) Hydridogermane und—silane: Synthese und Studien zur Abscheidung nanodimensionierter Materialien. PhD Thesis: Universität Bielefeld
- [48] Dittmar K, Jutzi P, Schmalhorst J, Reiss G (2001) Cyclopentadienyl germanes as novel precursors for the CVD of thin germanium films. *Chem Vap Deposition* 7:193
- [49] Woelk E, Shenai-Khatkhate DV, DiCarlo RL et al (2006) Designing novel organogermanium OMVPE precursors for high-purity germanium films. *J Cryst Growth* 287:684

- [50] Winkler C (1887) Mittheilungen über das Germanium. *J Prakt Chem* 36:177
- [51] Marshall AF, Thombare SV, McIntyre PC (2015) Crystallization pathway for metastable hexagonal close-packed gold in germanium nanowire catalysts. *Cryst Growth Des* 15:3734
- [52] Wang DW, Chang YL, Wang Q et al (2004) Surface chemistry and electrical properties of germanium nanowires. *J Am Chem Soc* 126:11602
- [53] Martino GD, Michaelis FB, Salmon AR, Hofmann S, Baumberg JJ (2015) Controlling nanowire growth by light. *Nano Lett* 15:7452
- [54] Meng Z, Jin Z, Gururaj BA, Chu P, Kwok HS, Wong M (1997) Germanium thin film formation by low-pressure chemical vapor deposition. *J Electrochem Soc* 144:1423
- [55] Nolan BM, Chan EK, Zhang X, Muthuswamy E, van Bentem K, Kauzlarich SM (2016) Sacrificial silver nanoparticles: reducing GeI_2 To form hollow germanium nanoparticles by electroless deposition. *ACS Nano* 10:5391
- [56] Carolan D, Doyle H (2015) Size controlled synthesis of germanium nanocrystals: effect of Ge precursor and hydride reducing agent. *J Nanomater.* 1:1–9
- [57] Henderson EJ, Seino M, Puzzo DP, Ozin GA (2010) Colloidally stable germanium nanocrystals for photonic applications. *ACS Nano* 4:7683
- [58] Bianco E, Butler S, Jiang S, Restrepo OD, Windl W, Goldberger JE (2013) Stability and exfoliation of germanane: a germanium graphane analogue. *ACS Nano* 7:4414
- [59] Wu MX, Vanhoutte G, Brooks NR, Binnemans K, Fransaeer J (2015) Electrodeposition of germanium at elevated temperatures and pressures from ionic liquids. *Phys Chem Chem Phys* 17:12080
- [60] Hohn N, Hetzenecker AE, Giebel MA et al (2019) Amphiphilic diblock copolymer-mediated structure control in nanoporous germanium-based thin films. *Nanoscale* 11:2048
- [61] Dahlhaus J, Jutzi P, Frenck HJ, Kulisch W (1993) Pentamethylcyclopentadienyl-substituted silanes ($\text{Me}_5\text{C}_4\text{SiH}_3$ and $(\text{Me}_5\text{C}_4)_2\text{SiH}_2$ as precursors for low-temperature remote plasma-enhanced CVD of thin silicon nitride and silica films. *Adv Mater* 5:377
- [62] Fritzsche R, Ruffer T, Lang H, Mehring M (2017) Synthesis and characterization of $\text{GeH}_2\text{Cp}^*_2$ and its structural comparison with SiXHCp^*_2 ($\text{X}=\text{Cl}, \text{H}$) and $\text{SnCl}_2\text{Cp}^*_2$. *Main Group Met Chem* 40:1
- [63] Wojnowska M, Noltemeyer M, Füllgrabe H-J, Meller A (1982) Zur chemie von t-butylgermanium-halogeniden und—chalkogeniden. *J Organomet Chem* 228:229
- [64] Vepřek S, Prokop J, Glatz F, Merica R, Klingan FR, Herrmann WA (1996) Organometallic chemical vapor deposition of germanium from a cyclic germylene, 1,3-Di-tert-butyl-1,3,2-diazagermolidin-2-ylidene. *Chem Mater* 8:825
- [65] Morimoto A, Kataoka T, Kumeda M, Shimizu T (1984) Annealing and crystallization processes in tetrahedrally bonded binary amorphous semiconductors. *Philos Mag B* 50:517
- [66] Chik KP, Lim P-K (1976) Annealing and crystallization of amorphous germanium thin films. *Thin Solid Films* 35:45
- [67] Germain P, Zellama K, Squelard S, Bourgoin JC, Gheorghiu A (1979) Crystallization in amorphous germanium. *J Appl Phys* 50:6986
- [68] Kazimierski P, Tyczkowski J, Kozanecki M, Hatanaka Y, Aoki T (2002) Transition from Amorphous Semiconductor to Amorphous Insulator in Hydrogenated Carbon–Germanium Films Investigated by Raman Spectroscopy. *Chem Mater* 14:4694
- [69] Pantellides S, Zollner S (2002) Silicon-germanium carbon alloys: growth, properties and applications. Taylor & Francis, New York - London
- [70] Liang XH, Zhang QH, Lay MD, Stickney JL (2011) Growth of Ge nanofilms using electrochemical atomic layer deposition, with a “Bait and Switch” surface-limited reaction. *J Am Chem Soc* 133:8199
- [71] Shah VA, Rhead SD, Halpin JE et al (2014) High quality single crystal Ge nano-membranes for opto-electronic integrated circuitry. *J Appl Phys* 115:10
- [72] Jellison GE (1992) Optical functions of GaAs, GaP, and Ge determined by two-channel polarization modulation ellipsometry. *Opt Mater* 1:151
- [73] El Boucham J, Maury F, Morancho R (1998) Thermal decomposition mechanisms of tetraethylgermane in metal-organic chemical vapor deposition. *J Anal Appl Pyrolysis* 44:153
- [74] Gencarelli F, Vincent B, Souriau L et al (2012) Low-temperature Ge and GeSn chemical vapor deposition using Ge_2H_6 . *Thin Solid Films* 520:3211
- [75] R Fritzsche (2017) Einsatz von Methylcyclopentadienyl-substituierten Silanen und Germanen zur Synthese verbrückter Heterozyklen und zur Abscheidung von dünnen Germaniumschichten. PhD Thesis: Technische Universität Chemnitz. <https://nbn-resolving.org/urn:nbn:de:bsz:ch1-qua-osa-227710>

Publisher's Note Springer Nature remains neutral with regard to jurisdictional claims in published maps and institutional affiliations.